Geometries and Electronic Properties of the Neutral and Charged Rare Earth Yb-Doped Si_n ($n = 1-6$) Clusters: A Relativistic Density Functional Investigation

Run-Ning Zhao,[†] Zhao-Yu Ren,[*,†] Ping Guo,[†] Jin-Tao Bai,[†] Chong-Hui Zhang,[†] and Ju-Guang Han[‡]

Institute of Photonics & Photon-Technology, Northwest University, Xian 710069, People's Republic of China, and Department of Chemistry and Biochemistry, Montana State University, Bozeman, Montana 59717

Received: September 29, 2005; In Final Form: January 23, 2006

The neutral and charged $YbSi_n$ ($n = 1-6$) clusters considering different spin configurations have been systematically investigated by using the relativistic density functional theory with generalized gradient approximation. The total bonding energies, equilibrium geometries, Mulliken populations (MP), Hirshfeld charges (HC), fragmentation energies, and highest occupied molecular orbital−lowest unoccupied molecular orbital (HOMO−LUMO) gaps are calculated and discussed. The optimized geometries indicate that the most stable $YbSi_n$ ($n = 1-6$) clusters keep basically the analogous frameworks as the low-lying Si_{n+1} clusters, while the charged species deviate from their neutral counterparts, and that the doped Yb tends to occupy the substitutional site of the neutral and charged $YbSi_n$ isomers. The relative stabilities are investigated in terms of the calculated fragmentation energies, exhibiting enhanced stabilities for the remarkably stable neutral and charged $YbSi_2$ and $YbSi_5$ clusters. Furthermore, the calculated MP and HC values show that the charges of the neutral and charged $YbSi_n$ clusters transfer from the Yb atom to Si_n atoms and the Yb atom acts as an electron donor, and that the f orbitals of the Yb atom in the neutral and charged $YbSi_n$ clusters behave as core without involvement in chemical bonding. The calculated HOMO−LUMO gaps indicate that the $YbSi_2$ and $YbSi_4^+$ clusters have stronger chemical stabilities. Comparisons of the Yb-doped Si_n ($n = 1-6$) with available theoretical results of transition-metal-doped silicon clusters are made. The growth pattern is investigated also.

1. Introduction

Silicon clusters have attracted great attention and have been studied extensively by using both theoretical and experimental techniques,[1−21] as they may be employed not only as model systems for investigating localized effects in the condensed phase, but also as building blocks for developing new silicon-based nanomaterials with tunable properties. However, pure silicon clusters are unsuitable as the building blocks, because they are chemically reactive due to the existence of dangling bonds.[12−17] Transition metal atom-doped silicon clusters, on the other hand, may tend to form closed-shell electronic structures that are of higher stability than the pure species and represent a new class of endohedral clusters encapsulating metal atoms.

The pioneering experimental work on $TMSi_n$ (TM = Cu, Cr, Mo, and W) clusters shows that the TM-doped silicon clusters are relatively more stable toward photofragmentation than the bare silicon clusters of the similar size.[18] Recently, Hiura et al.[19] had reported experimental evidence of the stable metal-encapsulated silicon cluster ions of MSi_n (M = Hf, Ta, W, Re, Ir; $n = 14, 13, 12, 11, 9$) and proposed a regular hexagonal prism WSi_{12} model with the W atom being encapsulated into the Si_{12} frame. The geometric and electronic properties of terbium−silicon anions, $TbSi_n^-$ ($6 \le n \le 16$),[20] were studied by using photoelectron spectroscopy and a chemical-probe method; the experimental results of the electron affinities (EAs) combined with data on the adsorption reactivity toward H_2O show that the Tb atom was encapsulated inside the Si_n cage at $n \ge 10$. Very recently, the photoelectron spectra of the chromium-doped silicon cluster anions, $CrSi_n^-$ ($n = 8-12$),[21] were measured; experimental results on vertical detachment energies indicate that the $CrSi_{12}$ unit has enhanced stability with the chromium atom being encapsulated inside the Si_{12} cage. Having been stimulated by these experiment observations, several computational investigations were performed for TM-doped silicon clusters;[22−35] the calculated results indicate that the TM in the lowest-energy $TMSi_n$ geometries occupied a gradual sinking site, and the site varies from the TM surface-absorbed forms to the TM-encapsulated forms with the size of the Si_n atoms increasing. Moreover, the charge transfer between the TM atom and the Si_n framework depends on different kinds of TM and cluster size, and the stabilities for the specific-sized TM−silicon clusters have been enhanced after the TM is doped into the Si_n frame.

Rare earth compounds are used as catalysts in the production of petroleum and synthetic products, while rare earth silicides improve the strength and workability of low-alloy steels. In a way, rare earths are special transition metals, possessing many of the properties of these elements (such as optical property, magnetism, and so forth). However, rare earths have distinctive chemical and physical properties. Moreover, the magnetic effects of the different electrons in the incomplete 4f subshell do not cancel each other as they do in a completed subshell, giving rise to strong magnetism. The saturation moments of some rare earth elements are greater than those of iron, cobalt, and nickel.[36] Although the YbO, YbF, YbH, and YbS dimers have been investigated theoretically,[37−40] surely no experimental or theoretical investigation on the neutral and charged rare earth $YbSi_n$

* To whom correspondence should be addressed. E-mail: rzy@nwu.edu.cn.
[†] Northwest University.
[‡] Montana State University.

10.1021/jp055551w CCC: $33.50
Published on Web 03/02/2006

($n = 1-6$) clusters has been reported so far. To reveal the unusual properties of the rare-earth-doped silicon clusters, the main objective of this research, therefore, is to provide a detailed investigation of equilibrium geometries, charge-transfer properties, relative stabilities, fragmentation energies [$D(n, n-1)$], atomic averaged binding energies [$E_b(n)$], ionization potentials (IPs), electron affinities (EAs), and HOMO−LUMO gaps of $YbSi_n$ clusters, which can provide instrumental help in the quest for this type of cluster-assembled material. However, it should be pointed out that the optimization of the rare earth Yb-doped Si_n is a challenging problem when the number of isomers increases significantly with the cluster size.

2. Computational Details

2.1. Relativistic Effects. Relativistic effects were treated by two different approaches: (i) the quasi-relativistic formalism (Pauli), and (ii) the zeroth-order regular approximation (ZORA). The quasi-relativistic formalism proceeds from a first-order perturbation approach based upon the Pauli Hamiltonian H^{Pauli} (eq 1, in atomic units). The latter is obtained from the Dirac Hamiltonian by the procedure of elimination of the small components, followed by an expansion, up to first order, of the resulting operator in $(E - V)/2c^2$ and some manipulations.[41,42]

$$H^{\text{Pauli}} = V + \frac{p^2}{2}\frac{p^4}{8c^2}\frac{\Delta V}{8c^2} + \frac{1}{4c^2}\vec{\sigma}\cdot(\Delta V \times \vec{p}) \qquad (1)$$

The first two terms of H^{Pauli} (the potential V and kinetic energy operator $p^2/2$) represent the nonrelativistic Hamiltonian and, in fact, correspond to an expansion up to only zeroth order. The last three terms can be conceived as a first-order relativistic perturbation, consisting of the so-called mass−velocity term $p^4/8c^2$ (a correction to the kinetic energy associated with the relativistic increase of the electron's mass), the Darwin term $\Delta V/8c^2$ (a correction to the effective potential associated with the so-called Zitterbewegung of the electron), and the spin−orbit operator (which couples electron spin and orbital moments). In the present study, only the scalar relativistic effects are taken into accounts, i.e., the spin−orbit operator is not included. In the Pauli approach, the relativistic energy correction is obtained through diagonalizing the first-order relativistic operator (i.e., the relativistic terms in H^{Pauli}) in the space of zeroth-order solutions (i.e., the nonrelativistic MOs). This turns out to improve calculated results significantly over a simple first-order perturbation treatment. Nevertheless, the Pauli treatment suffers from a series of problems.

Most of the problems associated with the Pauli Hamiltonian and the Pauli approach can be solved if the Hamiltonian resulting from elimination of the small components is expanded in $1/(2c^2 - V)$ instead of $(E - V)/2c^2$. To the zeroth order, this leads to the ZORA Hamiltonian (eq 2, in atomic units). So, our zeroth-

$$H^{\text{ZORA}} = \vec{\sigma}\cdot\vec{p}\,\frac{c^2}{2c^2 - V}\vec{\sigma}\cdot\vec{p} + V \qquad (2)$$

order Hamiltonian is not the nonrelativistic Hamiltonian. In fact, it is expected to incorporate relativistic effects that are traditionally only introduced at the Pauli Hamiltonian level. The great advantage of H^{ZORA} is that it may be used variationally and does not suffer from the singularities for $r \to 0$ that plague the Pauli Hamiltonian. Therefore, the ZORA relativistic approach is often superior (compared with the Pauli and nonrelativistic (NR) DFT) and in other cases at least similar to the older Pauli method. In particular for all-electron calculations generally and for heavy elements even within the frozen-core approach, the Pauli method may exhibit significant shortcomings. This is mostly due to the variational instability of the Pauli formalism in the deep-core region near the nucleus. The ZORA approach does not suffer from these problems and is, thus, highly recommended over the Pauli formalism.[41,42]

2.2. Computational Approach. All geometry optimizations and properties are calculated by utilizing the Amsterdam Density Functional package (ADF 2004.01),[43] which can perform the density functional theory (DFT) calculations of atoms, molecules, and clusters. The relativistic effects are of importance because the neutral and charged $YbSi_n$ clusters involve a heavy rare-earth element (Yb). A combined scalar or spin−orbit relativistic (SR) zeroth-order regular approximation (ZORA)[41,42] has been taken into account, and a frozen-core triple-ζ basis set plus polarization function (TZP) is employed for the neutral and charged $YbSi_n$ clusters. However, the comparison of the bonding energies of the neutral and charged $YbSi_n$ clusters at the scalar relativistic and spin−orbit approximations, respectively, show that the application of the spin−orbit operator simultaneously lowers the bonding energy by approximately 0.16 eV; therefore, the spin−orbit coupling effect was not considered for having no effect substantively on total bonding energies of the neutral and charged $YbSi_n$ clusters. For the ytterbium and silicon atoms, the intershell orbitals are kept frozen up to the 5p and 2p subshells, respectively. Except where explicitly stated, all calculations are based on the local density approximation[44] (LDA) augmented with the Becke−Perdew's exchange and correlation functionals.[45,46]

For each stationary point of a cluster, the stability is examined by calculating the harmonic vibrational frequencies. If an imaginary frequency is found, a relaxation along the coordinates of the imaginary vibrational mode is carried out until a true local minimum is reached. Therefore, geometries and total bonding energies for each stable cluster and its stable isomers correspond to the local minima. However, as the number of isomers increases quickly with the cluster size, it is very difficult to determine the global minimum simply according to the calculated energies of the isomers. To find the most stable $YbSi_n$ ($n = 1-6$) clusters as one possibly can, one considers first some previous theoretical or experimental results that are available; second, the equilibrium geometry is obtained by varying the geometry starting from high-symmetry structure to low-symmetry structure. Meanwhile, the spin electron configurations of $YbSi_n$ are restricted from $S = 0$, to 1, and to 2, and the harmonic vibrational frequencies of the lowest-energy isomers in three electron spin configurations were calculated. In addition, the influence of the additional charge on the geometries, stabilities, and total bonding energies of $YbSi_n$ clusters was examined by relaxing all neutral isomers.

To test the reliability of our calculations, the Si_2, Yb_2, and YbF molecules are, respectively, carried out; and their bond lengths, vibrational frequencies, and dissociation energies are illustrated in Table 1. The calculated results of the Si_2, Yb_2, and YbF clusters are in good agreement with the reported experimental results.[47,48]

3. Results and Discussions

3.1. Geometry and Stability. The equilibrium geometries of the neutral and charged $YbSi_n$ ($n = 1-6$) clusters are displayed in Figure 1, in which the cutoff distances of the Yb−Si and Si−Si bonds are defined as 3.10 and 2.70 Å, respectively. On the basis of the relative stabilities starting from low energies to high energies, different isomers are designated by *n*a, *n*b,

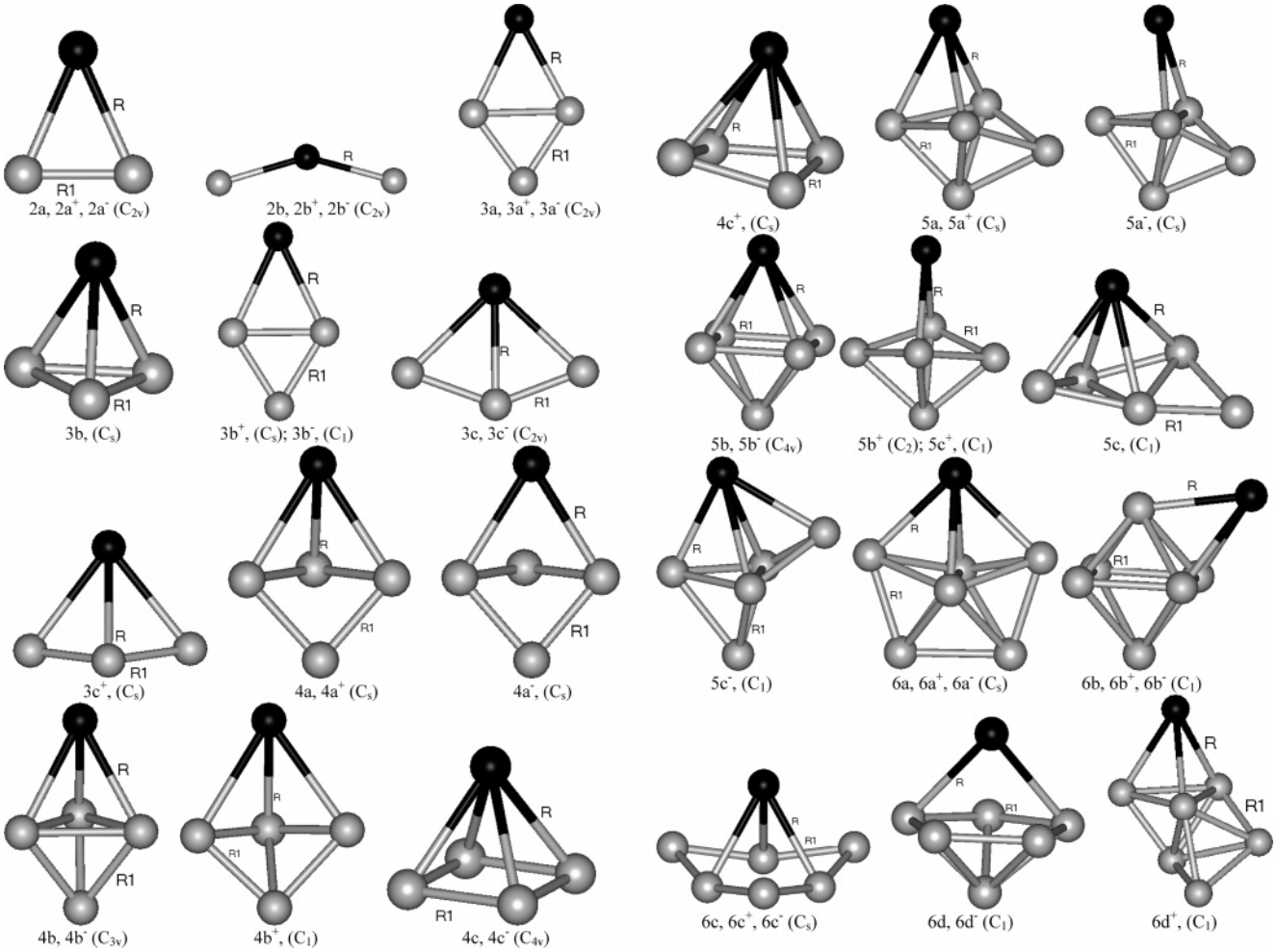

Figure 1. The equilibrium geometries of the neutral and charged $YbSi_n$ ($n = 1-6$) clusters.

TABLE 1: Bond Length (R), Vibratonal Frequency (ω_e), and Dissociation Energy (D_e) for the Ground Electronic State

molecule	method	electronic state	R (Å)	ω_e (cm^{-1})	D_e (eV)
Si_2	DFT	$^3\Sigma_g^-$	2.306	463.5	3.30
	exptl[a]	$^3\Sigma_g^-$	2.246	510.98	3.21
Yb_2	DFT	$^1\Sigma$		33.4	0.12
	exptl[b]	$^1\Sigma$		33	0.17
YbF	DFT	$^2\Sigma^+$	2.021	503.92	4.96
	exptl[a]	$^2\Sigma^+$	2.016	501.91	4.80

[a] ref 47. [b] ref 48.

*n*c, and so on; a corresponds to the lowest-energy isomer, *n* is the number of Si atoms in $YbSi_n$ clusters, and (+) and (−) denote the corresponding $YbSi_n^+$ and $YbSi_n^-$ clusters, respectively. Geometries, point-group symmetries, electronic states, and total bonding energies of $YbSi_n$, $YbSi_n^+$, and $YbSi_n^-$ ($n = 1-6$) clusters are listed in Table 2.

YbSi. The equilibrium geometries of the $C_{\infty v}$ YbSi dimer with electronic spin configurations of $S = 0$, 1, and 2 are optimized, together with the harmonic frequency analysis. The total bonding energies of the YbSi cluster with spin $S = 0$, 1, and 2 are −1.686, −2.351, and −1.406 eV, respectively, indicating that the triplet isomer is lower in total bonding energy than the singlet and quintet isomers by 0.665 and 0.945 eV, respectively. Therefore, the triplet YbSi dimer is a ground state; the corresponding electronic state is $^3\Sigma^+$. This feature is similar to those of the MoSi,[25] WSi,[27] and NiSi;[32] however, it differs from those of the previous TMSi (TM = Ir, Ta, Re, Zr, Sc, Cu, and Fe).[28−31,33,34] The bond length of the triplet YbSi isomer is 2.806 Å, which is longer than the TM−Si bond length of TMSi (TM = Mo, Cr, W, Ir, Ta, Re, Zr, Ni, Sc, Cu, and Fe),[25−34] reflecting that the Yb−Si interaction is much weaker than the TM−Si interaction.

When comparing the triplet YbSi geometry with those of $YbSi^+$ and $YbSi^-$ dimers, it is obvious that the Yb−Si bond length of YbSi is shorter than those of $YbSi^+$ and $YbSi^-$ isomers by 0.168 and 0.138 Å, respectively, indicating that the removal or addition of charge to the YbSi dimer will lead to an elongation of the Yb−Si bond.

$YbSi_2$. The possible $YbSi_2$ geometries such as C_{2v}, $C_{\infty v}$, and $D_{\infty h}$ isomers with spin configurations considered are optimized. The closed isosceles triangle (C_{2v} 2a) and the open isosceles triangle (C_{2v} 2b) are identified for the $YbSi_2$ clusters (Figure 1); their electronic states are described as $^1A_1$ and $^5A_1$, respectively (Table 2). However, the C_{2v} 2b is obviously higher in total bonding energy than the C_{2v} 2a isomer. According to the calculated results, it is found that the total bonding energies of the stable C_{2v} 2a cluster are increased as the spin goes from $S = 0$ to $S = 2$ monotonically; therefore, the singlet $YbSi_2$ 2a cluster is lower in total bonding energy than those of the triplet and quintet C_{2v} 2a isomers. In addition, the linear $C_{\infty v}$ cluster with electronic spin configurations of $S = 0$, 1, and 2 is not a stable structure. On the basis of the calculated total bonding energies, it is confirmed that the singlet C_{2v} $YbSi_2$ (2a) is the most stable structure and a ground state (Table 2); this finding is different from the most stable triplet $ZrSi_2$,[31] $NiSi_2$,[32] and $FeSi_2$[34] isomers, but it is identical to the singlet $TMSi_2$ (TM = Mo, Cr, and W)[25−27] isomers.

TABLE 2: Geometries, Point-Group Symmetries, Electronic States, and Total Bonding Energies of Neutral and Charged $YbSi_n$ ($n = 1-6$) Clusters[a]

		neutral			cation			anion		
cluster	isomer	sym	state	E_T (eV)	sym	state	E_T (eV)	sym	state	E_T (eV)
YbSi	1a	$C_{\infty v}$	$^3\Sigma^+$	−2.3513	$C_{\infty v}$	$^2\Pi$	4.0215	$C_{\infty v}$	$^4\Sigma^-$	−3.4009
$YbSi_2$	2a	C_{2v}	$^1A_1$	−7.3439	C_{2v}	$^2A_1$	−0.8687	C_{2v}	$^2A_1$	−8.6638
	2b	C_{2v}	$^5A_1$	−4.5685	C_{2v}	$^4B_2$	2.0430	C_{2v}	$^6B_1$	−6.5123
$YbSi_3$	3a	C_{2v}	$^1A_1$	−11.9915	C_{2v}	$^2A_1$	−5.4987	C_{2v}	$^2A_1$	−13.5292
	3b	C_s	$^1A'$	−11.2395	C_s	$^2A'$	−5.4984	C_1	^2A	−13.5281
	3c	C_{2v}	$^3B_1$	−10.8245	C_s	$^2A''$	−4.9168	C_{2v}	$^4B_1$	−12.7348
$YbSi_4$	4a	C_s	$^1A'$	−16.2676	C_s	$^2A'$	−9.9217	C_s	$^2A'$	−18.2019
	4b	C_{3v}	$^3A_1$	−15.9380	C_1	^2A	−9.8883	C_{3v}	$^4A_1$	−17.6341
	4c	C_{4v}	$^5A_1$	−15.0766	C_s	$^4A'$	−9.5109	C_{4v}	$^6A_1$	−16.8419
$YbSi_5$	5a	C_s	$^1A'$	−21.8922	C_s	$^2A'$	−15.5100	C_s	$^2A'$	−23.8197
	5b	C_{4v}	$^3A_1$	−21.4105	C_2	^2B	−15.5145	C_{4v}	$^4A_1$	−23.0912
	5c	C_1	^1A	−20.4723	C_1	^2A	−15.5139	C_1	^2A	−23.4456
$YbSi_6$	6a	C_s	$^1A'$	−26.2984	C_s	$^2A'$	−20.1978	C_s	$^2A'$	−28.2911
	6b	C_1	^1A	−25.6459	C_1	^2A	−19.6172	C_1	^2A	−27.8141
	6c	C_s	$^1A'$	−25.6456	C_s	$^2A'$	−18.9649	C_s	$^2A'$	−27.6699
	6d	C_1	^3A	−25.5852	C_1	^2A	−19.8401	C_1	^4A	−27.1965

[a] Sym represents symmetry; state represents electronic state; E_T denotes the total bonding energy of neutral and charged $YbSi_n$ clusters.

As for the charged clusters, the calculated results proved that the doublet $YbSi_2^+$ and $YbSi_2^-$ are the most stable isomers; furthermore, it is observed that the Yb−Si bond lengths in the doublet $YbSi_2^+$ (2.833 Å) and $YbSi_2^-$ (2.928 Å) are slightly longer than in the singlet $YbSi_2$ (2.747 Å) cluster, while the Si−Si bond lengths in the doublet $YbSi_2^+$ (2.159 Å) and $YbSi_2^-$ (2.183 Å) clusters are shorter than in the singlet $YbSi_2$ (2.216 Å) cluster because of an extra charge, and the ∠SiYbSi bond angles in the $YbSi_2^+$ (44.8°) and $YbSi_2^-$ (43.8°) clusters are smaller than in the $YbSi_2$ (47.6°).

$YbSi_3$. The previous theoretical results on the ground-state rhombus D_{2h} Si_4 clusters with electronic state of ^1A_g were a guide.[5−7] The three $YbSi_3$ isomers (Figure 1) emerging from substituting the Yb atom for one of the Si atoms in the D_{2h} Si_4 cluster or capping the Yb impurity into various adsorption sites of C_{2v} Si_3 cluster[7] are lowered to C_{2v} or C_s symmetries upon geometric relaxations. Moreover, all isomers are confirmed to be the local minima on the respective potential energy surfaces by aid of the calculated vibrational frequency analyses.

As shown in Figure 1, the rhombus C_{2v} $YbSi_3$ (3a) structure can be regarded as one Si atom being capped on the bottom of the C_{2v} $YbSi_2$ (2a) cluster or the Yb atom replacing one Si atom on the long diagonal of D_{2h} Si_4 cluster. The Yb atom substituting one of the Si atoms in the short diagonal of D_{2h} Si_4 cluster leads to a new rhombus $YbSi_3$ (3c) structure. Interestingly, the two rhombic structures, which have identical C_{2v} symmetry, can be found as different isomers with different ∠Si−Y−Si bond angles. As seen from Table 2, the $YbSi_3$ (3a) is more stable than the 3c isomer in that the $YbSi_3$ 3c isomer is higher in total bonding energy than the $YbSi_3$ 3a by 1.167 eV. Furthermore, the new Cs 3b isomer, which is formed with one Yb atom being face-capped on the planar Si_3 cluster, is higher in total bonding energy by 0.752 eV than the $YbSi_3$ 3a isomer. In addition, the computational results reveal that the Y-like D_{3h} isomer with Yb atom being inserted into the center site of the Si_3 frame is an unstable structure. Consequently, the C_{2v} 3a with singlet spin configuration is selected as the most stable structure and the ground state; the corresponding electronic state is $^1A_1$. It should be pointed out that the equilibrium geometry of the most stable $YbSi_3$ 3a cluster is similar to those of the rhombus $TMSi_3$ (TM = Cr, Ni, Sc, and Cu)[26,32,33] clusters.

The charged $YbSi_3$ ($3a^+$ and $3b^+$) clusters, which can be depicted as rhombus-like structures (Figure 1), essentially maintain the analogous framework of the neutral 3a $YbSi_3$ cluster upon addition or removal of one charge. However, the remarkable Yb−Si bond lengths in $3a^+$ are slightly shorter, while all Yb−Si bond lengths in $3a^-$ are longer in comparison to the neutral 3a isomer. However, all Si−Si bond lengths in $3a^+$ and $3a^-$ are longer than in 3a. Unexpectedly, the additional charge on the planar $3b^+$ and $3b^-$ clusters causes a serious distortion of the neutral C_s 3b geometry, and furthermore, the changes in geometry lead to a difference of 0.7976 eV between the vertical and adiabatic ionization potentials as well as a large difference of 0.8772 eV between the vertical and adiabatic electron affinities (Table 3). For the charged 3c structure, the $3c^-$ cluster deviates slightly from the neutral 3c geometry; on the contrary, the $3c^+$ structure has a significant distortion of the corresponding neutral counterparts (Figure 1).

TABLE 3: Atomic Averaged Binding Energies E_b of Neutral and Charged $YbSi_n$ Clusters, Vertical Ionization Potentials and Adiabatic Ionization Potentials, as Well as Vertical Electron Affinities and Adiabatic Electron Affinities of the $YbSi_n$ Clusters

		E_b (eV)			AIP	VIP	AEA	VEA
cluster	isomer	neutral	cation	anion	(eV)	(eV)	(eV)	(eV)
YbSi	1a	0.7563	0.7374	0.0091	6.3728	6.4261	1.0496	1.0233
$YbSi_2$	2a	1.8901	1.8434	1.3920	6.4752	6.5263	1.3199	1.2191
	2b	0.9650	0.8728	0.4668	6.6115	6.6368	1.9438	1.8613
$YbSi_3$	3a	2.3708	2.3313	1.9972	6.4928	6.5953	1.5377	1.3666
	3b	2.1828	2.3313	1.8092	5.7411	6.5387	2.2886	1.4114
	3c	2.0790	2.1859	1.7054	5.9077	6.1200	1.9103	1.8559
$YbSi_4$	4a	2.5849	2.5827	2.2860	6.3459	6.5251	1.9343	1.8569
	4b	2.5190	2.5760	2.2201	6.0497	7.0652	1.6961	1.5315
	4c	2.3467	2.5005	2.0478	5.5657	6.1862	1.7653	1.6253
$YbSi_5$	5a	2.9524	2.9445	2.7033	6.3822	6.6059	1.9275	1.7364
	5b	2.8721	2.9453	2.6230	5.8960	6.4422	1.6807	1.5218
	5c	2.7157	2.9452	2.4667	4.9584	6.3056	2.9733	1.9646
$YbSi_6$	6a	3.0408	3.0743	2.8273	6.1006	6.1487	1.9927	1.8583
	6b	2.9476	2.9913	2.7341	6.0287	6.2410	2.1682	2.0492
	6c	2.9475	2.8982	2.7341	6.6807	6.7563	2.0243	1.8695
	6d	2.9389	3.0232	2.7254	5.7451	6.8012	1.6113	1.5052

$YbSi_4$. A variety of possible geometries are optimized initially for the $YbSi_4$ clusters. It should be pointed out that the Yb-centered T_d isomer and planar C_{2v} isomers with spin $S = 0$, 1, and 2 turn out to be the unstable structures. At last, the three stable isomers are identified for the $YbSi_4$ (Figure 1). Both C_s 4a and C_{3v} 4b isomers can be described as trigonal bipyramidal structures, and the stable singlet C_s $YbSi_4$ (4a) cluster with electronic state of $^1A'$ is obtained by face-capping one silicon atom on the most stable C_{2v} $YbSi_3$ cluster. The stable triplet C_{3v} 4b isomer, which is obtained by replacing the apex Si atom

of the D_{3h} Si_5 cluster[7] with a Yb atom, can be viewed as one silicon atom being capped on the bottom of the pyramidal $YbSi_3$ 3b also. The former is more stable than the latter in that the former is lower in total bonding energy by 0.3296 eV than the latter. Finally, the tetragonal pyramid quintet $YbSi_4$ 4c structure ($^5A_1$) with the Yb atom interacting with four Si atoms directly, which can be described as the Yb impurity surface-absorbed D_{4h} Si_4 square,[7] is higher in total bonding energy than the C_s 4a isomer by 1.191 eV. Therefore, the singlet C_s 4a is the most stable structure. In addition, the framework of the singlet C_s $YbSi_4$ is similar to those of the $MoSi_4$,[25] $ZrSi_4$,[31] and $NiSi_4$ clusters.[32] Meanwhile, the framework of the most stable $YbSi_4$ 4a deviates strongly from those of $TMSi_4$ (TM = Cr, W, Ir, and Cu)[26−28,33] clusters.

The influence of an extra charge to the three neutral $YbSi_4$ isomers is examined. Interestingly, the geometries of the three neutral $YbSi_4$ clusters are similar to those of the corresponding anionic clusters; for the cationic $4a^+$ species, the shortest Yb−Si and Si−Si bond lengths in the trigonal bipyramidal C_s 4a structure are elongated. Because of the extra positive charge, however, the $4b^+$ and $4c^+$ geometries are relaxed very much as compared to the neutral 4b and 4c clusters; moreover, the $4b^+$ structure with C_{3v} symmetry undergoes significant distortions into a more stable structure of low C_1 symmetry. It is worth pointing out that some Yb−Si and Si−Si bond lengths of this $4b^+$ structure are shortened, while a Si−Si bond in the middle triangle is broken, and that the $4b^+$ volume becomes incompact. Furthermore, the geometric variation from the 4b to the $4b^+$ leads to a large difference of 1.0155 eV between the vertical and adiabatic ionization potential (Table 3). In addition, all Yb−Si bond lengths of the distorted quadrangle pyramid $4c^+$ become longer, while all Si−Si bond lengths of the $4c^+$ become shorter than those of the neutral 4c cluster, and the whole structure becomes compact. For the anionic species, the Yb−Si and Si−Si bond lengths in the $4a^-$ isomer are influenced by the additional negative charge as compared with the 4a clusters. Additionally, the geometries of the $4b^-$ and $4c^-$ are obviously compact (Figure 1).

$YbSi_5$. Guided by the equilibrium geometries of $YbSi_3$ and $YbSi_4$ clusters, we found that the surface-capped geometries are apparently the dominant structures. Three possible $YbSi_5$ isomers being selected as the ground-state candidates are considered, which are depicted as the face-capped trigonal bipyramidal C_s 5a isomer, the tetragonal bipyramidal C_{4v} 5b isomer, and the edge-capped trigonal bipyramidal C_1 5c isomer (Figure 1). The C_s $YbSi_5$ (5a) is obtained by face-capping one silicon atom on the side of the C_s $YbSi_4$ cluster. In addition, a tetragonal bipyramidal C_{4v} $YbSi_5$ (5b) structure is born after one Si atom is capped on the bottom of the C_{4v} $YbSi_4$ (4c) isomer or the apex Si atom of the octahedron D_{4h} Si_6 cluster is replaced by a Yb atom;[7] the calculated results exhibit that the triplet C_{4v} 5b structure is a stable isomer. As far as the C_1 5c isomer is concerned, one finds that the low-symmetry stable C_1 5c isomer significantly distorts the initial C_{5v} geometry. As seen from Table 2, the 5a ($^1A'$) isomer is lower in total bonding energy than the 5b ($^3A_1$) and 5c (^1A) isomers; therefore, the singlet C_s $YbSi_5$ (5a) isomer is selected as the ground state. Although it is different from $TMSi_5$ (TM = Mo, W, Ir, Ta, Re, and Fe) isomers in geometry,[25,27−30,34] the equilibrium geometry of the $YbSi_5$ 5a isomer is consistent with those of $TMSi_5$ (TM = Zr, Ni, Sc, and Cu).[31−33]

As far as the cationic clusters are concerned, the $5a^+$ structure keeps the analogous framework as its neutral, and the Yb−Si and Si−Si bond lengths are changed as compared to its neutral. Interestingly, the $5b^+$and $5c^+$ structures have analogous geometries, which can be depicted as the Yb atom being edge-capped on the trigonal bipyramidal Si_n clusters. Furthermore, the $5b^+$ is slightly lower by 0.0045 and 0.0006 eV in total bonding energy than the $5a^+$ and $5c^+$ isomers, respectively (Table 2). In addition, the significant distortions of $5b^+$ and $5c^+$ geometries induce different energy orders of all the cationic species, namely, the new energy order is $5b^+$, $5c^+$, and $5a^+$, which is different from that of the corresponding neutral species (5a, 5b, and 5c). Therefore, the $5b^+$ isomer is the most stable cationic structure among all the isomers considered. This finding indicates that the energy orders and geometries of $YbSi_5^+$ clusters are influenced significantly by the extra positive charge.

For the anionic species, the $5a^-$ geometry has very little distortion of the 5a isomer, and the $5b^-$ geometry maintains basically the framework of the neutral 5b isomer. However, the $5c^-$ geometry has a large rearrangement of the neutral and turns into the Yb face-capped trigonal bipyramidal structure (Figure 1). The deviation of the anionic geometries results in the large difference of 1.009 eV between the vertical electron affinity (VEA) and adiabatic electron affinity (AEA) (Table 3).

$YbSi_6$. Starting from various initial structures, the $YbSi_6$ clusters are calculated by considering different spin configurations. Four isomers are identified for the $YbSi_6$, which are the compressed pentagonal bipyramidal C_s 6a isomer, the distorted face-capped octahedron 6b isomer, the boatlike 6c isomer, and the pentagonal bipyramidal C_1 6d isomer (Figure 1).

The initial geometry with the Yb-encapsulated Si_6 octahedron is considered; however, the final optimized structure reveals that the Yb atom in the $YbSi_6$ isomer moves from the center site of the Si_6 frame to the surface site of the Si_6 frame, or in other words, there is no low-lying state where the Yb atom can be encapsulated into the Si_6 octahedron. As observed from the optimized geometries and energies, the lowest-energy isomer is a compressed pentagonal bipyramidal $YbSi_6$ 6a structure, which can be obtained by capping one Si atom on the most stable C_s $YbSi_5$ (5a) isomer at an appropriate site or by optimizing the substitutional structure after substituting a Yb impurity for one of the equatorial Si atoms in the D_{5h} Si_7 ($^1A'_1$) isomer.[7] In addition, the Yb surface-absorbed D_{4h} Si_6 isomer[7] results in a stable C_1 6b structure, which is higher in total bonding energy by 0.653 eV than the $YbSi_6$ 6a isomer. The C_s 6c isomer can be seen as one Yb atom being surface-capped on the distorted D_{3d} Si_6 cluster[7] and interacting with all six Si atoms simultaneously with nonequivalent bond lengths. It should be mentioned that the C_1 6b and C_s 6c isomers are the degenerated structures in energy. The C_{5v} 6d isomer is obtained with the Yb atom substituted for the apical Si atom of the most stable D_{5h} Si_7 cluster.[6−8] However, the vibrational frequency analysis confirms that the C_{5v} 6d structure has a negative frequency. A new stable C_1 6d structure is yielded after a slight distortion of the C_{5v} 6d geometry. Moreover, the calculated total bonding energy shows that the triplet C_1 6d isomer is more stable than the singlet and quintet C_1 6d structures.

According to the calculated total bonding energies of $YbSi_6$ isomers, the C_s $YbSi_6$ (6a) isomer with singlet spin configuration, which is tabulated in Table 2, is the lowest-energy structure and the ground state; the corresponding electronic state is $^1A'$. In comparison with the most stable $TMSi_6$[25−34] clusters, the geometry of the C_s $YbSi_6$ (6a) is in good agreement with those of the WSi_6,[27] $TaSi_6$,[29] and $ScSi_6$,[33] which maintain basically the framework of the most stable Si_7 cluster.[7]

The four anionic isomers ($6a^-$−$6d^-$) as well as cationic $6a^+$, $6b^+$, and $6c^+$ forms investigated nearly maintain the analogous

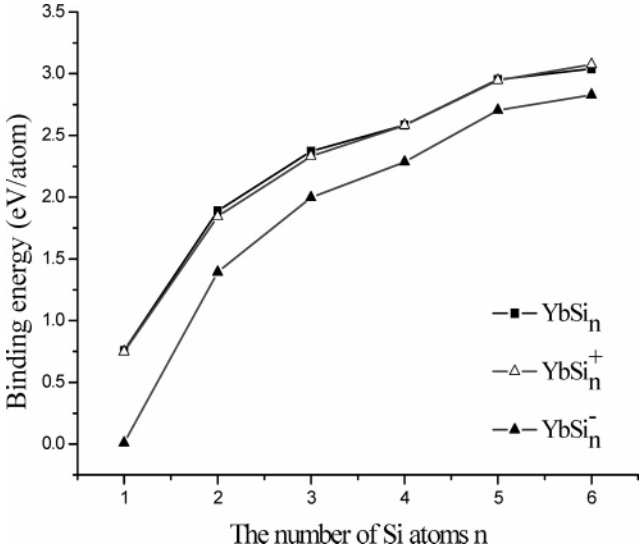

Figure 2. Size dependence of the atomic binding energy of the most stable neutral and charged $YbSi_n$ clusters

geometries of the corresponding neutral species, while the $6d^+$ deviates from its neutral geometry (Figure 1); the variation in geometry results in a large difference of 1.056 eV between the adiabatic ionization potential (AIP 5.745 eV) and the vertical ionization potential (VIP 6.801 eV) (Table 3).

3.2. Binding Energies and Fragmentation Energies. To investigate the relative stabilities of the most stable neutral and charged $YbSi_n$ ($n = 1-6$) clusters, it is significant to calculate the atomic-averaged binding energies ($E_b(n)$) with respect to the isolated atoms and fragmentation energies ($D(n, n-1)$) with respect to removal of one Si atom from the neutral and charged $YbSi_n$ clusters, which are shown in Figures 2 and 3 and Table 3. The atomic-averaged binding energies and fragmentation energies of the neutral and charged $YbSi_n$ ($n = 1-6$) clusters are defined as

$$E_b(YbSi_n) = \frac{E_T(Yb) + nE_T(Si) - E_T(YbSi_n)}{n+1}$$

$$E_b(YbSi_n^+) = \frac{E_T(Yb^+) + nE_T(Si) - E_T(YbSi_n^+)}{n+1}$$

$$E_b(YbSi_n^-) = \frac{E_T(Yb) + (n-1)E_T(Si) + E_T(Si^-) - E_T(YbSi_n)}{n+1}$$

$$D(n, n-1) = E_T(YbSi_{n-1}) + E_T(Si) - E_T(YbSi_n)$$

$$D(n, n-1) = E_T(YbSi_{n-1}^+) + E_T(Si) - E_T(YbSi_n^+)$$

$$D(n, n-1) = E_T(YbSi_{n-1}^-) + E_T(Si) - E_T(YbSi_n^-)$$

where $E_T(YbSi_{n-1})$, $E_T(YbSi_{n-1}^+)$, $E_T(YbSi_{n-1}^-)$, $E_T(Si)$, $E_T(Si^-)$, $E_T(Yb)$, $E_T(Yb^+)$, $E_T(YbSi_n)$, $E_T(YbSi_n^+)$, and $E_T(YbSi_n^-)$ denote the total bonding energy of the $YbSi_{n-1}$, $YbSi_{n-1}^+$, $YbSi_{n-1}^-$, Si, Si^-, Yb, Yb^+, $YbSi_n$, $YbSi_n^+$, and $YbSi_n^-$ clusters, respectively. The calculated results of the most stable neutral, cationic, and anionic $YbSi_n$ ($n = 1-6$) isomers are plotted as the curves of $E_b(n)$ and $D(n, n-1)$ against the corresponding number of Si atoms (Figures 2 and 3). The features of the size evolution are intuitively viewed, and the peaks of the curves correspond to those clusters having enhanced local stabilities.

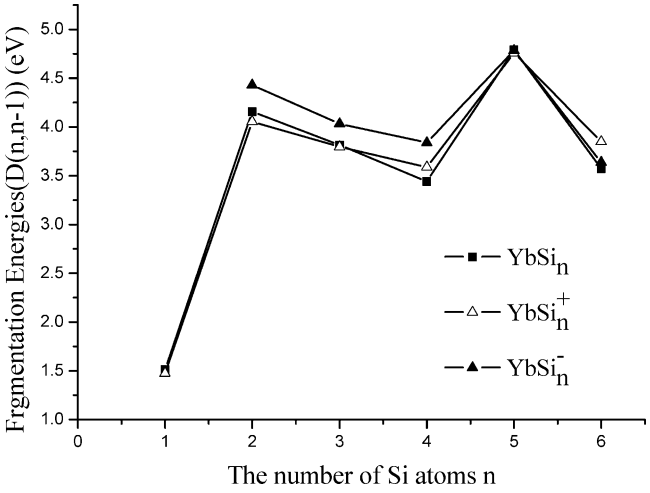

Figure 3. Size dependence of the fragmentation energies for the most stable neutral and charged $YbSi_n$ clusters.

Next, the size dependence of the atomic binding energies for the neutral and charged $YbSi_n$ forms is compared. It can be seen from Figure 2 that the atomic-averaged binding energies generally increase as the size of the neutral and charged $YbSi_n$ ($n = 1-6$) clusters increases. However, the curve for the atomic averaged binding energy of $YbSi_n^-$ is universally lower than those of $YbSi_n$ and $YbSi_n^+$ clusters, indicating that the stabilities of $YbSi_n$ and $YbSi_n^+$ clusters are stronger than for the corresponding $YbSi_n^-$; it is surprising that the stabilities of $YbSi_n$ clusters agree well with those of the $YbSi_n^+$ clusters. This feature of $YbSi_n$ is similar to those of $TMSi_n$ ($n = 1-6$) (TM = Ta, Sc, and Cu).[29,33] Unfortunately, the atomic-averaged binding energies deviate from the reliable relative stabilities.

According to the calculated fragmentation energies shown in Figure 3, two remarkable peaks at $n = 2$ and $n = 5$ are found for the neutral and charged $YbSi_n$ ($n = 1-6$) clusters, showing that the corresponding clusters have slightly stronger relative stabilities and have large abundances in mass spectroscopy as compared to the corresponding neighbors. In addition, the curves vary synchronously for the neutral and charged $YbSi_n$ forms, reflecting that the relative stabilities of the neutral and charged $YbSi_n$ vary synchronously with the cluster size.

3.3. Population Analysis. In the Hirshfeld method, a hypothetical promolecule with electron density $\Sigma\rho_B$ is constructed by the superposition of spherically symmetrized charge densities ρ_B of the isolated atoms B. The electron density ρ of the real molecule at each point in space is then distributed over the atoms A in the same ratio $W_A = (\rho_A/\Sigma\rho_B)$, as they contribute charge density to that point in the promolecule. The Hirshfeld atomic charge Q_A^H is obtained by subtracting the resulting partial density associated with the A atom from the corresponding nuclear charge Z_A (eq 3). The Hirshfeld scheme accounts in a natural way for the fact that each type of atom has a certain, characteristic effective size.[49]

$$Q_A^H = Z_A - \int W_A(r)\,\rho(r)\,dr^3 \qquad (3)$$

As compared with the Mulliken population method, the Hirshfeld method yields the atomic charges which are essentially stable against basis set variations and correctly reflect the electronegativity differences between the atoms. The Hirshfeld is a more satisfactory method with regard to the computation of chemically meaningful and basis set independent atomic charges. Therefore, the Hirshfeld analysis is even more recommended in the ADF program.[49,50]

TABLE 4: Net Mulliken Population (MP) and Hirshfeld Charge (HC) of Yb Atom for the Most Stable Neutral and Charged $YbSi_n$ Clusters

		neutral			cation			anion		
cluster	isomer	sym	MP	HC	sym	MP	HC	sym	MP	HC
YbSi	1a	$C_{\infty v}$	0.2979	0.3020	$C_{\infty v}$	0.7709	0.8302	$C_{\infty v}$	−0.2983	−0.3166
$YbSi_2$	2a	C_{2v}	0.3623	0.4998	C_{2v}	0.7819	0.9243	C_{2v}	−0.1728	−0.0676
$YbSi_3$	3a	C_{2v}	0.3862	0.4764	C_{2v}	0.7824	0.9115	C_{2v}	−0.0724	−0.0245
$YbSi_4$	4a	C_s	0.4201	0.5582	C_s	0.7693	0.8904	C_s	0.0389	0.1172
$YbSi_5$	5a	C_s	0.4901	0.5859	C_s	0.7397	0.8630	C_s	0.0736	0.1132
$YbSi_6$	6a	C_s	0.5229	0.6213	C_s	0.7281	0.8639	C_s	0.1112	0.1150

TABLE 5: Gross Orbital Population of Yb Atom of the Most Stable $YbSi_n$ Clusters

				gross orbital population			
cluster	isomer	symmetry	spin	6s	5d	6p	4f
YbSi	1a	$C_{\infty v}$	1	1.3942	0.3135	0.1417	13.8525
$YbSi_2$	2a	C_{2v}	0	1.0550	0.5962	0.1470	13.8396
$YbSi_3$	3a	C_{2v}	0	1.1324	0.4718	0.1586	13.8508
$YbSi_4$	4a	C_s	0	0.9690	0.6424	0.1582	13.8104
$YbSi_5$	5a	C_s	0	0.9104	0.5984	0.1472	13.8540
$YbSi_6$	6a	C_s	0	0.6570	0.8098	0.1852	13.8252

The net Mulliken populations (MP) and Hirshfeld charges (HC) of the Yb atom in the most stable neutral and charged $YbSi_n$ isomers are listed in Table 4; both the MP and HC populations for the most stable neutral and charged $YbSi_n$ isomers draw a consistent conclusion. The net MP and HC values for the Yb atom in the $YbSi_n$ and $YbSi_n^+$ ($n = 1-6$) clusters are positive (Table 4), showing that the charges in the corresponding clusters transfer from the Yb to the Si_n atoms. In addition, the net MP and HC values of the Yb atom in the $YbSi^-$, $YbSi_2^-$, and $YbSi_3^-$ clusters are negative, while the values for Yb in the $YbSi_4^-$, $YbSi_5^-$, and $YbSi_6^-$ clusters are positive. Furthermore, the MP and HC values of the Yb atom in the cationic clusters are bigger than those in the neutrals, and they are smaller than those in the anionic clusters (Table 4). These findings indicate that the Yb atom of the $YbSi_n^-$ ($n = 1-6$) clusters still loses electrons, while the net MP and HC values for the Yb atom in the $YbSi^-$, $YbSi_2^-$, and $YbSi_3^-$ are negative because of distribution of the additional negative charge. Gross orbital populations of the $YbSi_n$ ($n = 1-6$) clusters are summarized at Table 5, indicating that the charges in the $YbSi_n$ ($n = 1-6$) clusters mainly transfer from the 6s orbitals of the Yb atom and the 3s orbitals of the Si atoms to the 5d orbitals of the Yb atom and the 3p orbitals of the Si atoms.

According to the calculated atomic orbital populations of the most stable neutral $YbSi_n$ ($n \neq 3$), it obviously manifests that the orbital populations of the 6s subshells in the Yb atom are decreased, while the 5d orbital populations of the Yb atom are increased as the cluster size increases. The calculated orbital populations for the charged isomers show that the removed charge in the $YbSi_n^+$ mainly comes from the rare-earth Yb atom and the additional charge in the $YbSi_n^-$ is distributed on the Si_n frame. In addition, the f orbitals of the Yb atom in the neutral and charged $YbSi_n$ isomers behave as core without involvement in the chemical bonding; furthermore, the Yb atom in the most stable charged isomers acts as a donor of charges. Similar behaviors are observed in the $TMSi_n$ (TM = Ta, Zr, Ni, Sc, and Cu)[29,31−33] clusters. On the contrary, the charges in the $TMSi_n$ (TM = Mo, Cr, W, Ir, and Re)[25−28,30] clusters transfer from the Si_n atoms to the TM atom; the TM acts as an acceptor of charge.

3.4. AIP, VIP, AEA, and VEA. The adiabatic ionization potential (AIP), the vertical ionization potential (VIP), the adiabatic electron affinity (AEA), and the vertical electron affinity (VEA) are calculatedas defined in the following:

$$\mathrm{AIP} = E_T(\text{optimized } YbSi_n^+) - E_T(\text{optimized } YbSi_n)$$

$$\mathrm{VIP} = E_T(\text{nonoptimized } YbSi_n^+) - E_T(\text{optimized } YbSi_n)$$

$$\mathrm{AEA} = E_T(\text{optimized } YbSi_n) - E_T(\text{optimized } YbSi_n^-)$$

$$\mathrm{VEA} = E_T(\text{optimized } YbSi_n) - E_T(\text{nonoptimized } YbSi_n^-)$$

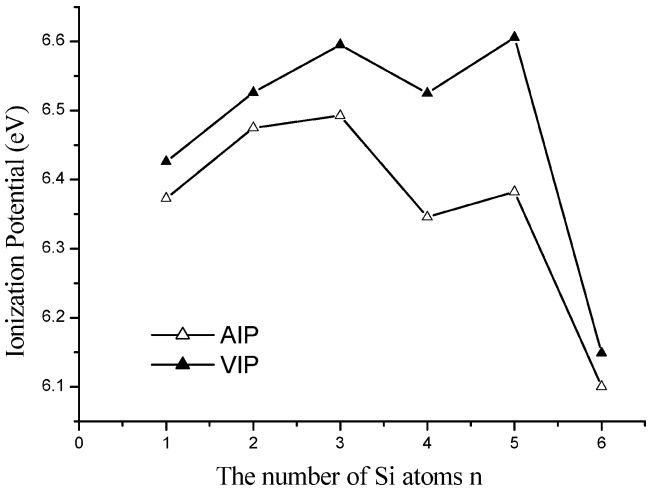

Figure 4. Size dependence of the vertical and adiabatic ionization potentials (VIP and AIP) for the most stable neutral and charged $YbSi_n$ clusters.

From Table 3, it is found that the differences in the calculated AIP and VIP as well as the AEA and VEA for the 1a, 2a, 2b, 3a, 3c, 4a, 5a, 6a, 6b, and 6c clusters are quite small; however, the differences between the AIP and VIP values for the $YbSi_n$ clusters, especially for the 3b, 4b, 4c, 5b, 5c, and 6d isomers, should be mentioned. This finding implies that greater or fewer geometric rearrangements exist when geometries vary from the neutral clusters to the cationic clusters. The two curves in Figure 4 show that the AIP and VIP values for the most stable $YbSi_n$ clusters are monotonically dependent on the cluster size and the VIP value is larger than the corresponding AIP value by about 0.04−0.23 eV, showing that the most stable $YbSi_n^+$ clusters basically keep the frameworks that are analogous to those of the corresponding most stable neutral clusters. However, there are several cases (3b, 4b, 4c, 5b, 5c, 6d) where the VIP values exceed the corresponding AIP data by about 0.54−1.35 eV (Figure 1), indicating that the considerable rearrangement in the corresponding geometries is associated with the removal of an electron from the neutral clusters. Furthermore, the $YbSi_6$ cluster has the lowest AIP, revealing that its cationic cluster is easily generated experimentally and corresponds to the enhanced abundance observed for this species in mass spectroscopy.

TABLE 6: Energies of the Highest Occupied Molecular Orbital (HOMO), the Lowest Unoccupied Orbital (LUMO), as well as the HOMO− LUMO Gaps of the Most Stable Neutral and Charged $YbSi_n$ ($n = 1-6$) Clusters

		neutral (eV)			cation (eV)			anion (eV)		
cluster	isomer	HOMO	LUMO	gap	HOMO	LUMO	gap	HOMO	LUMO	gap
YbSi	1a	−3.2028	−3.0239	0.1789	−8.9568	−8.8907	0.0661	1.4077	1.6894	0.2817
$YbSi_2$	2a	−3.4759	−3.0224	0.4535	−9.0242	−8.9154	0.1088	0.6969	0.9184	0.2215
$YbSi_3$	3a	−3.4140	−3.1508	0.2632	−8.8194	−8.7697	0.0497	0.5705	0.5706	0.0001
$YbSi_4$	4a	−3.8382	−3.6775	0.1607	−8.4970	−8.1542	0.3482	0.2511	0.2693	0.0182
$YbSi_5$	5a	−3.4670	−3.3131	0.1539	−8.3304	−8.2136	0.1168	0.1527	0.2179	0.0652
$YbSi_6$	6a	−3.4566	−3.2926	0.1640	−8.4763	−8.2400	0.2363	0.1681	0.2182	0.0501

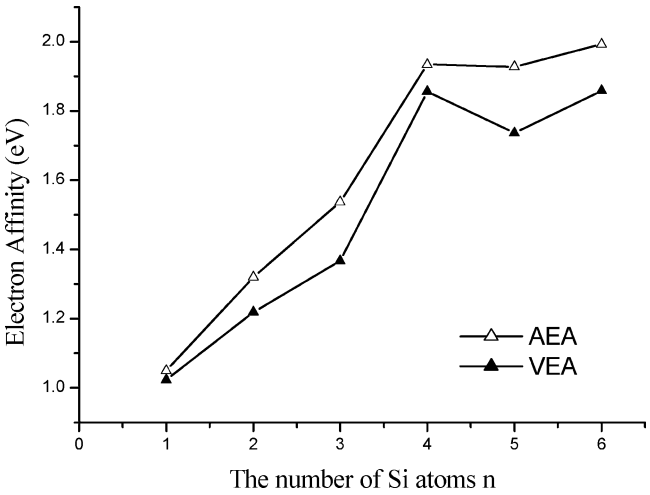

Figure 5. Size dependence of the vertical and adiabatic electron affinities (VEA and AEA) for the most stable neutral and charged $YbSi_n$ clusters.

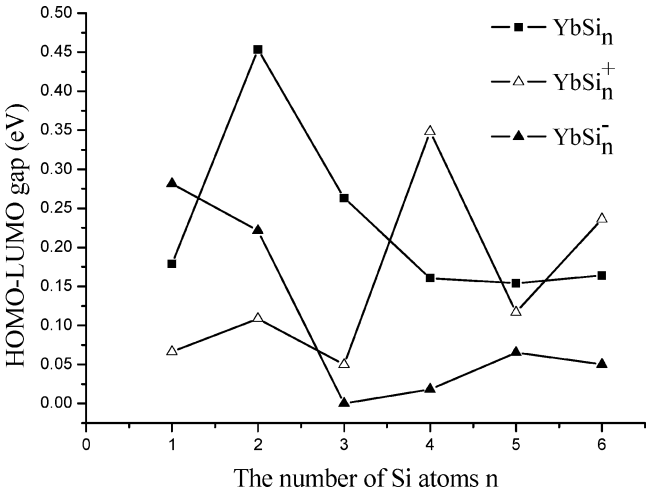

Figure 6. Size dependence of the HOMO−LUMO gaps for the most stable neutral and charged $YbSi_n$ clusters.

From Table 3, it is found that the differences between the AEA and the corresponding VEA values for the $YbSi_n$ clusters are rather small except for the 3b and 5c isomers, which show that a majority of the anionic clusters basically maintain the frameworks of the corresponding neutral clusters. The two curves of the size dependences of the AEA and VEA for the most stable $YbSi_n$ clusters are shown in Figure 5. The two curves have similar trends to a certain extent; however, small differences between the AEA and VEA by 0.02−0.20 eV exist. However, the 3b and 5c clusters with neutral and anionic forms have differences of 0.8772 and 1.0087 eV between the AEA and VEA, respectively, reflecting that the large arrangements of the 3b and 5c geometries resulting from the additional negative charge are obviously found when the 3b and 5c clusters vary from the neutral forms to anionic forms. In the other words, the additional negative charges of the $3b^-$ and $5c^-$ clusters cause obvious deformation of the original neutral clusters.

3.5. HOMO−LUMO Gap. The HOMO and LUMO energies as well as the corresponding HOMO−LUMO gaps of the neutral and charged $YbSi_n$ clusters are tabulated in Table 6. The HOMO and LUMO energies of the $YbSi_n^+$ clusters are universally lower than those of the corresponding $YbSi_n$ clusters, while the situation is reversed for the $YbSi_n^-$ (Table 6). Size dependence of the HOMO−LUMO gaps for the most stable neutral and charged $YbSi_n$ clusters are shown in Figure 6; it seems worthwhile to point out that the HOMO−LUMO gaps of the Si_{n+1} are bigger than those of the neutral and charged $YbSi_n$ clusters,[13] reflecting that the neutral and charged $YbSi_n$ and $TaSi_n$[29] clusters exhibit a universal narrowing of the HOMO−LUMO gap as compared to the pure silicon clusters[13] and the surfaced-capped Yb atoms in the neutral and charged $YbSi_n$ clusters obviously influence the HOMO−LUMO gaps of the original Si_{n+1} clusters; this finding shows that the chemical stabilities of the neutral and charged $YbSi_n$ clusters are decreased while the metallic characteristics of the neutral and charged $YbSi_n$ clusters should be strengthened when the Yb impurity is doped into Si_n clusters. It should be mentioned that the HOMO−LUMO gaps of the $YbSi_n^+$ and $YbSi_n^-$ clusters become smaller than those of the neutrals except for the three isomers $YbSi_4^+$, $YbSi_6^+$, and $YbSi^-$, and the chemical stability of the $YbSi_2$ and $YbSi_4^+$ clusters is improved dramatically as compared to the others.

4. Conclusions

A systematic investigation of the equilibrium geometries, stabilities, and electronic and bonding properties of the neutral and charged $YbSi_n$ ($n = 1-6$) clusters is performed by using a relativistic density functional theory (RDFT) with the generalized gradient approximation (GGA) considering the exchange-correlation energy. All calculated results can be summarized as follows.

(1) The most stable $YbSi_n$ ($n = 1-6$) clusters keep basically the frameworks analogous to the ground-state Si_{n+1} frames, and the Yb surface-capped $YbSi_n$ clusters are the dominant structures. This geometric feature is similar to that of the $ScSi_n$ ($n = 1-6$),[33] while it is incompletely consistent with those of $TMSi_n$ ($n = 1-6$) (TM = Mo, Cr, W, Ir, Ta, Re, Zr, Ni, Cu, and Fe).[25-34] Therefore, the growth pattern of metal-doped silicon clusters depends on the kind of doped metal.

(2) The influences of the positive or negative charge on the geometries and bonding energies of all $YbSi_n$ clusters are examined. In comparison with the neutral $YbSi_n$ clusters, the serious geometric deformations of the $3b^+$, $4b^+$, $4c^+$, $5b^+$, $5c^+$, and $6d^+$ geometries are exhibited, which are reflected by the differences between the respective VIPs and AIPs. As for $YbSi_n^-$, the considerable rearrangement of the $3b^-$ and $5c^-$ geometries leads to the large pronounced differences between the respective VEAs and AEAs.

(3) According to the calculated fragmentation energies of the neutral and charged $YbSi_n$ clusters, the relative stability is discussed. Theoretical results show that the marked small $YbSi_n$ ($n = 2, 5$) clusters with neutral and charged forms have enhanced stabilities as compared to the corresponding neighbors. Moreover, the relative stability of the neutral $YbSi_n$ ($n = 2, 5$) clusters agrees with the theoretical findings in the $ScSi_n$ and $CuSi_n$ ($n = 2, 5$).[33] Thus, it is expected that MSi_2 and MSi_5 (M =Yb, Sc, and Cu) could be produced in the mass spectrum with high relative abundance. In addition, the atomic averaged binding energies deviate from the reliable relative stabilities.

(4) Population analysis indicates that the charges in the $YbSi_n$ ($n = 1-6$) clusters mainly transfer from the 6s orbitals of the Yb atom and the 3s orbitals of the Si atoms to the 5d orbitals of the Yb atom and the 3p orbitals of the Si atoms. In addition, the f orbitals of the Yb atom behave as core without involvement in the chemical bonding. Generally, the charges for the neutral and charged $YbSi_n$ ($n = 1-6$) clusters transfer from Yb atom to Si atoms. The charge-transfer behavior is in good agreement with previous $TMSi_n$ (TM = Ta, Zr, Ni, Sc, and Cu) clusters,[29,31−33] but is opposite to the $TMSi_n$ ($n = 1-6$) with TM = Mo, Cr, W, Ir, and Re. [25−28,30.]

(5) The HOMO−LUMO gaps exhibit size and species dependence. As compared to pure silicon clusters, a universal narrowing of the HOMO−LUMO gap in the neutral and charged $YbSi_n$ clusters is revealed, which is consistent with that of $TaSi_n$.[29] Furthermore, The $YbSi_2$ and $YbSi_4^+$ clusters have enhanced chemical stability.

Acknowledgment. This work is supported by National Natural Science Foundation of China (cooperation item of west and east, grant no. 10247007); Natural Science Foundation of ShaanXi province (grant no. 2002A09); Special Item Foundation of Educational Committee of ShaanXi province (grant no. 02JK050); and National Natural Science foundation of P. R. China (grant nos. 20173055, 90206033).

References and Notes

(1) Koyasu, K.; Akutsu, M.; Mitsui, M.; Nakajima, A. *J. Am. Chem. Soc.* **2005**, *127*, 4998.
(2) Jarrold, M. F. *Science* **1991**, *252*, 1085.
(3) Bloomfield, L. A.; Freeman, R. R.; Brown, W. L. *Phys. Rev. Lett.* **1985**, *54*, 2246.
(4) Bloomfield, L. A.; Guesic, M. E.; Freeman, R. R.; Brown, W. L. *Chem. Phys. Lett.* **1985**, *121*, 33.
(5) Li, S.; Van Zee, R. J.; Weltner, W., Jr.; Raghavachari, K. *Chem. Phys. Lett.* **1995**, *243*, 275.
(6) Raghavachari, K.; Logovinsky, V. *Phys. Rev. Lett.* **1985**, *55*, 2853.
(7) Raghavachari, K. *J. Chem. Phys.* **1986**, *84*, 5672.
(8) Raghavachari, K.; Rohlfing, C. M. *J. Chem. Phys.* **1988**, *89*, 2219.
(9) Kaxiras, E.; Jackson, K. *Phys. Rev. Lett.* **1993**, *71*, 727.
(10) Rothlisberger, U.; Andreoni, W.; Parrinello, M. *Phys. Rev. Lett.* **1994**, *72*, 665.
(11) Yoo, S.; Zhao, J. J.; Wang, J. L.; Zeng, X. C. *J. Am. Chem. Soc.* **2004**, *126*, 13845.
(12) Ho, K.-M.; Shvartsburg, A. A.; Pan, B.; Lu, Z.-Y.; Wang, C.-Z.; Wacker, J. G.; Fye, J.; Jarrold, M. F. *Nature (London)* **1998**, *392*, 582.
(13) Hagelberg, F.; Leszczynski, J.; Murashov, V. *THEOCHEM* **1998**, *454*, 209.
(14) Rata, I.; Shvartsburg, A. A.; Horoi, M.; Frauenheim, T.; Siu, K. W. M.; Jackson, K. A. *Phys. Rev. Lett.* **2000**, *85*, 546.
(15) Jarrold, M. F.; Bower, J. E. *J. Chem. Phys.* **1992**, *96*, 9180.
(16) Wang, J.; Han, J. G. *J. Chem. Phys*. **2005,** *123*, 244303**.**
(17) Menon, M.; Subbaswamy, K. R. *Chem. Phys. Lett.* **1994**, *219*, 219.
(18) Beck, S. M. *J. Chem. Phys.* **1989**, *90*, 6306.
(19) Hiura, H.; Miyazaki, T.; Kanayama, T. *Phys. Rev. Lett*. **2001**, *86*, 1733.
(20) Ohara, M.; Miyajima, K.; Pramann, A.; Nakajima, A.; Kaya, K. *J. Phys. Chem. A* **2002**, *106*, 3702.
(21) Zheng, W.; Nilles, J. M.; Radisic, D.; Bowen, K. H. *J. Chem. Phys.* **2005**, *122*, 071101.
(22) Han, J. G.; Shi, Y. Y. *Chem. Phys.* **2001**, *266*, 33.
(23) Hagelberg, F.; Yanov, I.; Leszczynski, J. *THEOCHEM* **1999**, *487***,** 183.
(24) Kumar, V.; Kawazoe, Y. *Phys. Rev. Lett.* **2001**, *87*, 045503.
(25) Han, J. G.; Hagelberg, F. *THEOCHEM* **2001**, *549*, 165.
(26) Han, J. G.; Hagelberg, F. *Chem. Phys.* **2001**, *263*, 255.
(27) Han, J. G.; Xiao, C.; Hagelberg, F. *Struct. Chem.* **2002**, *13*, 173.
(28) Han, J. G. *Chem. Phys*. **2003**, *286*, 181.
(29) Guo, P.; Ren, Z. Y.; Wang, F.; Bian, J.; Han, J. G.; Wang, G. H. *J. Chem. Phys*. **2004**, *121*, 12265.
(30) Han, J. G.; Ren, Z. Y.; Lu, B. Z. *J. Phys. Chem. A* **2004**, *108***,** 5100.
(31) Wang, J.; Han, J. G. *J. Chem. Phys*. **2005**, *123*, 064306.
(32) Ren, Z. Y.; Li, F.; Guo, P.; Han, J. G. *THEOCHEM* **2005**, *718*, 165.
(33) Xiao, C.; Abraham, A.; Quinn, R.; Hagelberg, F.; Lester, W. A., Jr. *J. Phys. Chem. A* **2002**, *106*, 11380.
(34) Mpourmpakis, G.; Froudakis, G. E.; Andriotis, A. N.; Menon, M. *Phys. Rev. B* **2003**, *68*, 125407.
(35) Han, J. G.; Hagelberg, F. *Comput. Lett.* **2005**, *1*, 230.
(36) Ronda, C. R.; Justel, T. Nikol, H. *J. Alloys Compd.* **1998**, *275*, 669.
(37) Wang, S. G.; Pan, D. K.; Schwarz, W. H. E. *J. Chem. Phys*. **1995**, *102*, 9296.
(38) Wang, S. G.; Schwarz, W. H. E. *J. Phys. Chem.* **1995**, *99*, 11687.
(39) Heiberg, H.; Gropen, O.; Laerdahl, J. K.; Swang, O.; Wahlgren, U. *Theor. Chem. Acc.* **2003**, *110*, 118.
(40) Melville, T. C.; Coxon, J. A. *J. Chem. Phys.* **2000**, *113*, 1771.
(41) Diefenbach, A.; Bickelhaupt, F. M. *J. Chem. Phys*. **2001,** *15*, 4030.
(42) van Lenthee, E.; Bearends, E. J.; Snijders, J. G. *J. Chem. Phys*. **1993**, *99*, 4597.
(43) Velde, G. Te.; Baerends, E. J. *J. Comput. Phys*. **1992**, *99*, 84.
(44) Vosko, S. H.; Wilk, L.; Nusair, Can, M. *J. Phy.* **1980**, *58*, 1200.
(45) Becke, A. D. *Phys. Rev. A* **1988**, *38*, 3098.
(46) Perdew, J. P.; Wang, Y. *Phys. Rev. B* **1986**, *33*, 8822; **1992**, *45*, 13244.
(47) Huber, K. P.; Herzberg, G. *Constants of Diatomic Molecules*; Van Nostrand Reinhold: New York, 1979.
(48) Guido, M.; Balducci, G. *J. Chem. Phys.* **1972**, *57*, 5611.
(49) Bickelhaupt, F. M.; van Eikema Hommes, N. J. R.; Fonseca Guerra, C.; Baerends, E. J. *Organometallics* **1996,** *15*, 2923.
(50) Wiberg, K. B.; Rablen, P. R. *J. Comput. Chem*. **1993,** *14*, 1504.